Energy and Buildings 133 (2016) 529–540

Contents lists available at ScienceDirect

Energy and Buildings

journal homepage: www.elsevier.com/locate/enbuild

Experimental and numerical analysis of desiccant wheels activated at low temperatures

F. Comino*, M. Ruiz de Adana

Departamento de Química-Física y Termodinámica Aplicada, Escuela Politécnica Superior, Universidad de Córdoba, Campus de Rabanales, Antigua Carretera Nacional IV, km 396, 14072 Córdoba, Spain

ARTICLE INFO

Article history:
Received 5 July 2016
Received in revised form 13 October 2016
Accepted 14 October 2016
Available online 14 October 2016

Keywords:
Desiccant wheel
Low temperature activated systems
Moisture removal capacity
Sensible heat ratio
Design of experiments

ABSTRACT

Desiccant wheels, DW, can be used to control the indoor air conditions in buildings and industrials environments. The control of the outlet process air conditions of a DW can be obtained by controlling the moisture removal capacity, MRC, and sensible heat ratio, SHR. The objective of this work is to obtain MRC and SHR of a DW activated at low temperatures when the process airflow rate and air regeneration temperature are varied. Two secondary objectives are to obtain the influence of the variation of the process airflow rate and air regeneration temperature on the outlet process air conditions and the relationship between MRC and SHR. Three empirical and simulated case studies are carried out.

The results show that a decoupling of the outlet air temperature and humidity ratio can be obtained when the process airflow rate and air regeneration temperature are varied. This decoupling allows several MRC values for a constant SHR value, and vice versa, to be obtained, achieving ranges of 7 kg h^{-1} and 0.25, respectively. These results suggest that a control strategy for DW activated at low temperatures, would allow MRC and SHR to be controlled by setting the process airflow rate and air regeneration temperature.

1. Introduction

Desiccant systems present an alternative solution to refrigeration vapour compression systems, commonly used for dehumidification and humidity control in rooms with high latent loads. Refrigeration vapour compression systems reduce the air temperature to condense its moisture, although these systems present some problems in the combined treatment of sensible and latent loads in rooms [1]. Furthermore, refrigeration vapour compression systems working under partial load conditions, presented a reduced latent capacity compared to nominal latent capacity [2]. Desiccant dehumidifier systems differ from refrigeration vapour compression systems in the way moisture is removed from the air. Desiccant dehumidifier systems adsorb water vapour from the air reaching an area of low vapour pressure at the surface of the desiccant [1]. These systems combined with refrigeration vapour compression systems, called hybrid HVAC systems, proved to be especially useful in the decoupling of sensible and latent loads in buildings [3,4].

In HVAC systems, control strategies are required to achieve the independent control of temperature and humidity. The aim of a control strategy is to improve the performance of the system, while satisfying user's thermal comfort [5]. Many HVAC systems based on DW using two-stage dehumidification achieved a fine tuning of humidity ratio [6–8]. However, this control would not guarantee independent control of temperature and humidity. Other HVAC systems with DW combined with a enthalpy wheel were studied to control indoor conditions [9]. This system did not have capacity to control indoor humidity during some critical periods.

Previous research studies on DW control strategies were carried out with the aim of saving energy by setting the regeneration section with a purge sector [10]. Another control strategy approach is based on the rotation speed of a DW [11,12]. The control system would be much more energy efficient using the variable airflow rate [13]. The rotation speed and the regeneration temperature were also used as a control strategy [14]. Nevertheless, these works have not satisfactorily clarified the capacity to decouple the outlet process air conditions, temperature and humidity ratio, especially as regards the quantitative effect of both variables.

Manufacturers often provide controls inside the system to modulate the reactivation energy of the DW in response to changes in the moisture load. There are three common methods of controlling dehumidification capacity [15]: (i) on-off reactivation control; (ii) reactivation energy modulation; and (iii) variable air bypass. Each of these methods is effective, depending on the degree of precision needed for the humidity control level in the building [15].

A schematic of a DW system with an air bypass is shown in Fig. 1. It requires a bypass air duct and variable-position dampers for the face of the DW and for the bypass duct. The DW would oper-

* Corresponding author.
E-mail address: francisco.comino@uco.es (F. Comino).

http://dx.doi.org/10.1016/j.enbuild.2016.10.021
0378-7788/

Nomenclature

A	Area [°C g kg^{-1}]
AR	Area ratio
b	Estimated parameter
CC	Cooling coil
DOE	Design of experiments
DW	Desiccant wheel
EA	Exhaust air
F	Centrifugal fan
FC	Flow conditioner
EH	Electric heater
HC	Heating coil
HR	Relative humidity [%]
K	Number of parameters
MA	Mixed air
MB	Mixing box
MRC	Moisture removal capacity [kg h^{-1}]
N	Number of experimental tests
OA	Outdoor air
P	Pressure [Pa]
PT	Pitot tube
$\dot{Q}$	Heat transfer [kW]
RA	Recirculated air
SH	Steam humidifier
SHR	Sensible heat ratio
T	Temperature [°C]
t	Time [s]
$\dot{V}$	Volumetric airflow rate [m^3 h^{-1}]
X	Input variable
$\hat{Y}$	Estimated output value

Greek letters

Δ	Increase
ρ	Density [kg m^{-3}]
ω	Humidity ratio [g kg^{-1}]
Ω	Specific mass airflow rate [kg s^{-1} m^{-3}]

Subscripts

d	Dew point
i	Inlet
L	Latent
o	Outlet
p	Process
r	Regeneration
S	Sensible

Superscripts

'	Mixed outlet process air conditions

ate with unbalanced airflow rates to achieve the outlet process air conditions. This method is preferred for industrial process applications, where control within ±1 or 2% relative humidity is essential [15]. Previous results also showed that if the outlet moisture must be very low, the process airflow rate is quite critical and therefore this must be controlled [1].

Different experimental works have been carried out in order to study the influence of unbalanced airflow rates in DW [16,17]. Other authors developed mathematical models of DW which allowed its behaviour with unbalanced airflow rates to be analysed [18,19]. However, the methodology used to fit these models requires a high number of experimental tests. Some physical characteristics of the DW required by these models are not usually available.

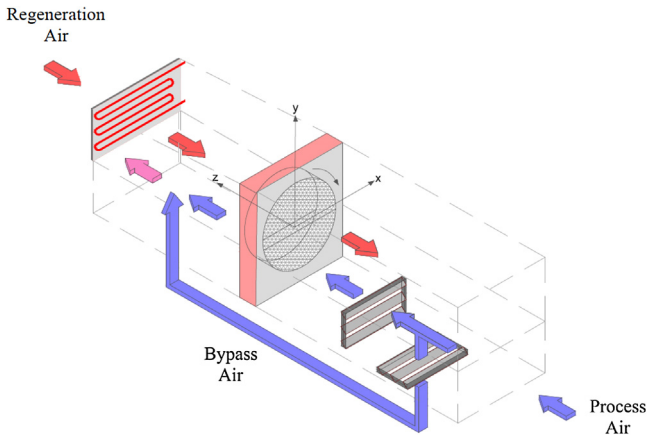

Fig. 1. Schematic of a DW system with bypass air.

It has been shown that the variation of process airflow rate allowed the psychrometric trend of the process air stream and moisture removal capacity, MRC, to be modified [20]. The psychrometric trend of the process air stream can be studied by sensible heat ratio, SHR, [21]. Several studies on HVAC systems with DW analysed SHR [22,23]. Nevertheless, to modify MRC the air regeneration temperature was more influential than the airflow rates [24].

MRC was considered to be the most appropriate parameter to analyse the performance of a DW with unbalanced airflow rates [25]. The higher the temperature of the desiccant material, the higher the MRC, and the easier it is to remove moisture. Thus, the regeneration air temperature has a strong effect on MRC [26,27]. Therefore, a significant energy consumption is required to regenerate the DW to obtain high MRC values. Energy savings are usually obtained when the DW is regenerated using waste heat from other processes [28]. However, in some cases waste heat energy is not available or the corresponding temperature level is not adequate. On the other hand, previous studies on DW operated at low regeneration temperatures and reached acceptable MRC values [29,30]. A DW activated at low temperatures could be integrated in refrigeration vapour compression systems in a building or industrial environment [31,32]. In this paper, values below 60 °C were considered as low regeneration temperatures. The regeneration temperatures usually used range from 60 °C to 120 °C [33,34].

The performance and the outlet process air conditions of a DW strongly depend on its control strategy. Therefore, it would be interesting to know the behaviour of a DW activated at low temperatures by setting the process airflow rate and air regeneration temperature, in order to control MRC and SHR.

The objective of this work was to obtain empirically MRC and SHR of a DW activated at low temperatures when the process airflow rate and air regeneration temperature were varied. To obtain this, two secondary objectives were carried out: first, to study the influence of the variation of the process airflow rate and air regeneration temperature on the outlet process air conditions, and then to obtain the relationship between MRC and SHR.

2. Methodology

2.1. Experimental setup

An experimental test rig was built to analyse the performance of DW under different working conditions. A schematic representation of the experimental setup is shown in Fig. 2. The process and regeneration air streams were configured in a countercurrent flow. The facility is also designed to bypass up to 40% of the process air

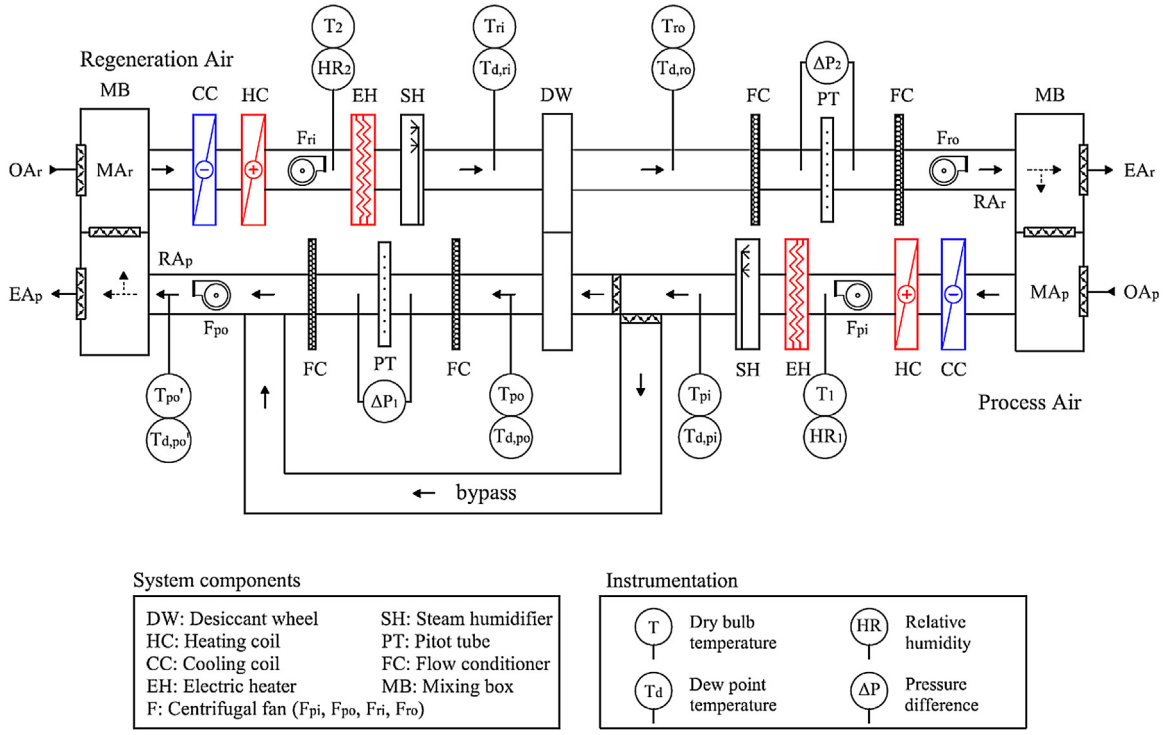

Fig. 2. Layout of the test facility.

stream without being treated by the DW. It has a bypass air duct and variable-position dampers for the face of the DW and for the bypass duct. The DW could operate with unbalanced airflow rates to achieve the outlet process air conditions.

The inlet temperature and humidity ratio of both process and regeneration streams were set using cooling and heating coils (CC, HC), an electric heater (EH) and a steam humidifier (SH), located for each air stream, upstream of the DW [35]. The process and regeneration airflow rates were set using variable speed fans (F). Two Pitot tubes (PT) were used to measure the airflow rate and four flow conditioners (FC) were installed to obtain stable airflow conditions, two upstream of the airflow rate measuring point and two downstream. Furthermore, two mixing boxes (MB), were used either to recirculate the process and regeneration air streams or to mix the exterior air with the treated air. The characteristics of the equipment of the test facility setup are shown in Table 1.

The DW is divided into two equal sections and rotates at a constant speed of 42 rph. The matrix of the DW consists of alternate layers of flat and corrugated sheets of silica gel and metal silicates, chemically bonded into a tissue of inorganic fibres. The dimensional sizes and operating parameters of the DW are shown in Table 2.

The measured variables in this test rig, the type of sensor and its accuracy are shown in Table 3. The sensor locations are shown in Fig. 2. The temperature and humidity at each measuring point were collected at three different points along the horizontal axis, taking the average of the three measurements [14].

Each state point was taken under steady-state conditions and all the measured values were average values over a period of 20 min with sampling time steps of 3 s [35]. The maximum values of standard deviations of the mean are shown in Table 4.

Table 1
Characteristics of the equipment.

Equipment	Value
Cooling coil (CC)	
Total cooling capacity	15.8 kW
Sensible cooling capacity	12.2 kW
Nominal water flow	2.7 $m^3 h^{-1}$
Nominal pressure drop	5.1 m
Heating coil (HC)	
Heating capacity	18.8 kW
Nominal water flow	2.7 $m^3 h^{-1}$
Nominal pressure drop	5.1 m
Electric heater (EH)	
Electric power	7.2 kW
Fan (F)	
Nominal airflow	3100 $m^3 h^{-1}$
Available static pressure	0.007 m
Nominal motor power	0.6 kW
Speed	1125 rpm
Steam humidifier (SH)	
Steam flow	45 kg h^{-1}
Max. power	33.75 kW

2.2. Design of experiments

The statistical technique of design of experiments, DOE, was used to fit an empirical regression model which was used to predict the outlet air process temperature and humidity ratio in the DW system with bypass air, T_{po}' and ω_{po}', showing a similar setting to Fig. 1. In addition, DOE allowed the influential variables on T_{po}' and ω_{po}' to be identified and analysed [36]. The number of required experimental tests can be reduced if they are optimally designed. Usually, several candidate models can be proposed. The choice between these candidate models is a trade-off between complexity and precision. The fit of the model and its further statistical analysis were supported by the software Statgraphics Centurion XVI [37].

In this work, a DOE was carried out with five input variables: inlet air process temperature, T_{pi}, inlet air process humidity ratio, ω_{pi}, process specific mass airflow rate, Ω_{pi}, ratio of inlet mass velocity to the channel length [38], inlet air regeneration temperature, T_{ri} and inlet air regeneration humidity ratio, ω_{ri}. The output process

Table 2
Characteristics of the desiccant wheel.

Parameters	Value
Rotor diameter	550 mm
Rotor length	200 mm
Desiccant material	Silica gel
Channel shape	Honeycomb
Nominal capacity	15 kg h^{-1}
Nominal air flow	2300 m^3 h^{-1}
Rotation speed	42 rph
Weight	57 kg
Power supply	230 Vac

Table 3
Specification of measuring devices.

Measured parameter	Type	Accuracy
T_1, T_2, T_{pi}, T_{po}, $T_{po'}$, T_{ri}, T_{ro}	PT 100	±0.12 °C
$T_{d,pi}$, $T_{d,po}$, $T_{d,po'}$	Chilled mirror hygrometer	±0.15 °C
$T_{d,ri}$, $T_{d,ro}$	Capacitive	±0.4 °C
HR_1, HR_2	Capacitive	±3%
ΔP_1, ΔP_2	Differential pressure transmitter	±0.3% (0–1 mbar)

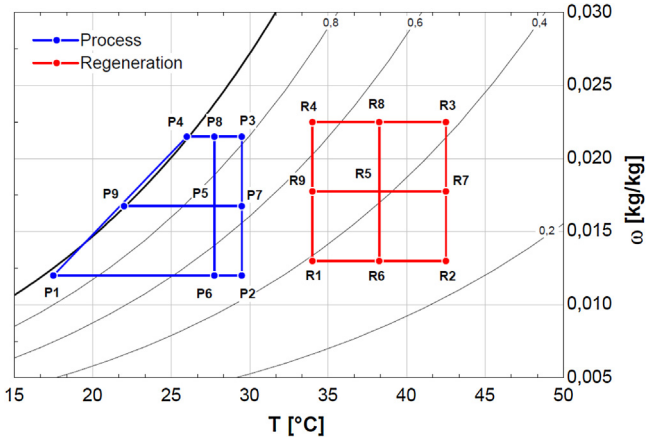

Fig. 3. Grid for the inlet states of the process and regeneration airflow.

variables were the outlet air process temperature of system, T_{po}', and outlet air process humidity ratio of system, ω_{po}'. The effect of the five input variables was studied using a Box-Behnken design approach [36]. This design was carried out at low air regeneration temperatures defining two grids to cover the range of validity of the process and regeneration air streams, as shown in Fig. 3. Nine inlet states for the process airflow, P1 to P9, and nine inlet states for the regeneration airflow, R1 to R9, were selected. The resulting process grid was not rectangular, in order to obtain the widest range of validity.

The values of the nine inlet states for the process and regeneration airflow are shown in Table 5. The inlet air process temperature ranged from 17.5 °C to 29.5 °C and the humidity range from 12 g kg^{-1} to 21.5 g kg^{-1}. Furthermore, the process specific mass airflow rate values were varied in three levels, 13.45 kg s^{-1} m^{-3} ($\Omega_{pi,1}$), 17.48 kg s^{-1} m^{-3} ($\Omega_{pi,2}$) and 21.51 kg s^{-1} m^{-3} ($\Omega_{pi,3}$). The inlet air regeneration temperature range was from 34 °C to 42.5 °C and the humidity range from 13 g kg^{-1} to 22.5 g kg^{-1}. The regeneration specific mass airflow rate was fixed at a constant value for all tests, 21.51 kg s^{-1} m^{-3}.

Table 5
Inlet states of the process and regeneration airflow.

Point	T_{pi} [°C]	ω_{pi} [g kg^{-1}]	Point	T_{ri} [°C]	ω_{ri} [g kg^{-1}]
P1	17.50	12.00	R1	34.00	13.00
P2	29.50	12.00	R2	42.50	13.00
P3	29.50	21.50	R3	42.50	22.50
P4	26.00	21.50	R4	34.00	22.50
P5	27.25	16.75	R5	38.25	17.75
P6	27.25	12.00	R6	38.25	13.00
P7	29.50	16.75	R7	42.50	17.75
P8	27.25	21.50	R8	38.25	22.50
P9	22.00	16.75	R9	34.00	17.75

Table 6
Experimental tests defined for DOE based on the Box-Behnken design approach.

N	Process	Regeneration	Ω_{pi}	N	Process	Regeneration	Ω_{pi}
1	P6	R5	$\Omega_{pi,1}$	24	P5	R6	$\Omega_{pi,3}$
2	P5	R2	$\Omega_{pi,2}$	25	P7	R5	$\Omega_{pi,1}$
3	P6	R7	$\Omega_{pi,2}$	26	P5	R8	$\Omega_{pi,3}$
4	P9	R8	$\Omega_{pi,2}$	27	P8	R5	$\Omega_{pi,3}$
5	P6	R6	$\Omega_{pi,2}$	28	P8	R7	$\Omega_{pi,2}$
6	P5	R6	$\Omega_{pi,1}$	29	P6	R9	$\Omega_{pi,2}$
7	P4	R5	$\Omega_{pi,2}$	30	P7	R9	$\Omega_{pi,2}$
8	P9	R7	$\Omega_{pi,2}$	31	P5	R8	$\Omega_{pi,1}$
9	P5	R5	$\Omega_{pi,2}$	32	P8	R9	$\Omega_{pi,2}$
10	P3	R5	$\Omega_{pi,2}$	33	P6	R5	$\Omega_{pi,3}$
11	P5	R5	$\Omega_{pi,2}$	34	P7	R8	$\Omega_{pi,2}$
12	P9	R5	$\Omega_{pi,1}$	35	P5	R5	$\Omega_{pi,2}$
13	P8	R8	$\Omega_{pi,2}$	36	P9	R9	$\Omega_{pi,2}$
14	P5	R4	$\Omega_{pi,2}$	37	P5	R7	$\Omega_{pi,1}$
15	P5	R5	$\Omega_{pi,2}$	38	P5	R9	$\Omega_{pi,3}$
16	P5	R5	$\Omega_{pi,2}$	39	P9	R6	$\Omega_{pi,2}$
17	P6	R8	$\Omega_{pi,2}$	40	P8	R5	$\Omega_{pi,1}$
18	P7	R6	$\Omega_{pi,2}$	41	P5	R5	$\Omega_{pi,2}$
19	P5	R9	$\Omega_{pi,1}$	42	P7	R7	$\Omega_{pi,2}$
20	P8	R6	$\Omega_{pi,2}$	43	P7	R5	$\Omega_{pi,3}$
21	P5	R1	$\Omega_{pi,2}$	44	P1	R5	$\Omega_{pi,2}$
22	P5	R3	$\Omega_{pi,2}$	45	P5	R7	$\Omega_{pi,3}$
23	P9	R5	$\Omega_{pi,3}$	46	P2	R5	$\Omega_{pi,2}$

A total of 46 experimental tests were carried out, including 6 repetitions of the tests combining the interior points, P5, R5 and $\Omega_{pi,2}$, and 25 degrees of freedom. The combination of tests are summarized in Table 6.

The performance of the process was evaluated by analysing the responses (Y), which are dependent on the input variables. The relationship between the responses and the input variables was examined using second order polynomial equations. The generalized second order polynomial equation model is expressed by Eq. (1). Where $\hat{Y}$ is the estimated output value, X are input variables, b_i, b_{ii} and b_{ij} are the estimated parameters of linear, quadratic and the second-order terms, respectively, and b_0 is the average response in the model.

$$\hat{Y} = b_0 + \sum_{i=1}^{k} b_i \cdot X_i + \sum_{i=1}^{k} b_{ii} \cdot X_i^2 + \sum_{i=1}^{k=1} \sum_{\substack{i=2 \\ j>i}}^{k} b_{ij} \cdot X_i \cdot X_j \quad (1)$$

In order to check if the selected model accurately describes the observed data, the R^2 value was obtained, and a lack-of-fit test of the model was carried out. This test was performed by comparing the

Table 4
Maximum values of standard deviations of the mean.

	T_{pi} [°C]	ω_{pi} [g kg^{-1}]	T_{po} [°C]	ω_{po} [g kg^{-1}]	T_{ri} [°C]	ω_{ri} [g kg^{-1}]	T_{ro} [°C]	ω_{ro} [g kg^{-1}]	$\dot{V}_p$ [m^3 h^{-1}]	$\dot{V}_r$ [m^3 h^{-1}]
Σ	0.17	0.46	0.34	0.50	0.31	0.53	0.21	0.42	28.2	24.7

Table 7
Experimental tests for case study I.

N	T_{pi} [°C]	ω_{pi} [g kg^{-1}]	Ω_{pi} [kg s^{-1} m^{-3}]	T_{ri} [°C]	ω_{ri} [g kg^{-1}]	Ω_{ri} [kg s^{-1} m^{-3}]
1	25.00	17.00	21.51	34.00	13.00	21.51
2	25.00	17.00	21.51	38.25	13.00	21.51
3	25.00	17.00	21.51	42.50	13.00	21.51
4	25.00	17.00	17.48	42.50	13.00	21.51
5	25.00	17.00	13.45	42.50	13.00	21.51
6	25.00	17.00	13.45	38.25	13.00	21.51
7	25.00	17.00	13.45	34.00	13.00	21.51
8	25.00	17.00	17.48	34.00	13.00	21.51

Table 8
Inlet air states of Ω_{pi}, T_{ri} and ω_{ri} for case study II.

Ω_{pi} [kg s^{-1} m^{-3}]	T_{ri} [°C]	ω_{ri} [g kg^{-1}]
13.45	34.00	13.00
17.48	38.25	17.75
21.51	42.50	22.50

variability of the current model residuals to the variability between observations at replicate settings of the factors.

2.3. Strategy to control outlet process air conditions

In this work, three case studies were carried out to analyse the outlet process air conditions of a DW when the inlet air regeneration temperature and process airflow rate were controlled. Case study I was tested experimentally and case studies II and III were carried out for different inlet air conditions using the empirical model fitted with the technique DOE. This technique allows to fit the model by using a low number of experimental tests. The analysis of the outlet process air conditions for a wide range of inlet air states was carried out using the empirical model.

2.3.1. Case study I

The decoupling potential of the outlet air process temperature and humidity ratio were evaluated in case study I by varying three levels of T_{ri} and three levels of Ω_{pi}, see Table 7. The remaining input variables were fixed at constant values. In order to quantify the decoupling of the outlet process air conditions of the DW, a psychrometric area, A_o, was obtained. The psychrometric area was calculated from the contour of the outlet process air states, where the main axes of psychrometric chart were considered the dry bulb temperature, horizontal axis, and the humidity ratio, vertical axis.

2.3.2. Case study II

In this case study five inlet process air conditions were defined, states P1-P5, see Fig. 3. The combination of three levels of T_{ri}, ω_{ri} and Ω_{pi} was used to analyse the outlet air process temperature, T_{po}', and the outlet air process humidity ratio, ω_{po}', see Table 8. Ω_{ri} was fixed at a constant value, 21.51 kg s^{-1} m^{-3}. The results of outlet process air conditions were quantified by the aforementioned variable A_o.

2.3.3. Case study III

In practice, inlet process air conditions could vary over time, for example, when these conditions are influenced by outdoor air. In order to analyse the outlet process air conditions of the DW system when inlet process air conditions vary, a third case study was performed. In this case, three inlet process air areas were selected. These areas are related to three climatic conditions, see Fig. 4:

- Area I: inlet process air conditions with low temperature and low humidity ratio values
- Area II: inlet process air conditions with high temperature values and low humidity ratio values

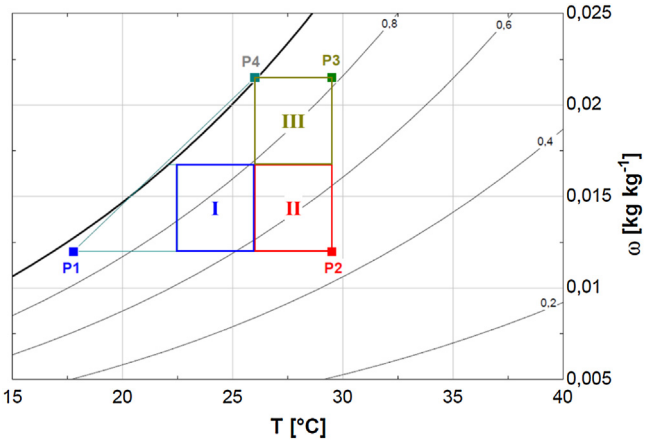

Fig. 4. Inlet process air condition areas considered for case study III.

- Area III: inlet process air conditions with high temperature and high humidity ratio values.

All areas have the same dimensions, 16.6 °C g kg^{-1}. The limit condition values of the process input areas are summarized in Table 9.

The outlet process air conditions of the DW system for variable inlet air conditions were quantified by an area ratio between outlet and inlet air area, AR, expressed by Eq. (2). The inlet and outlet air area values were obtained from the contour of the inlet air states and outlet air states, respectively.

$$AR = \frac{A_o}{A_i} \tag{2}$$

2.4. Moisture removal capacity and sensible heat ratio

In a DW, the variation of outlet air process humidity ratio, ω_{po}', from a given inlet air process humidity ratio, ω_{pi}, causes the desiccant capacity to be modified. Therefore, the moisture removal capacity, MRC, of the DW in the three case studies was obtained. ASHRAE defines MRC as a primary figure of merit for desiccant wheel performance [39]. MRC was defined as:

$$MRC = \rho \cdot \dot{V} \cdot \left(\omega_{pi} - \omega'_{po}\right) \tag{3}$$

Similar desiccant capacities in a DW are possible, so MRC was analysed regarding the sensible heat ratio, SHR, expressed by Eq. (4). Where $\dot{Q}_S$ is the sensible heat transfer of the process air stream and $\dot{Q}_L$ is the latent heat transfer of the process air stream. SHR values range between 0 and 1.

$$SHR = \frac{\dot{Q}_S}{\dot{Q}_S + \dot{Q}_L} \tag{4}$$

Table 9
Limit states of the inlet process air condition areas considered for case study III.

	Area I		Area II		Area III	
	T_{pi} [°C]	ω_{pi} [g kg^{-1}]	T_{pi} [°C]	ω_{pi} [g kg^{-1}]	T_{pi} [°C]	ω_{pi} [g kg^{-1}]
Lower limit	22.5	12	26	12	26	16.75
Upper limit	26	16.75	29.5	16.75	29.5	21.5

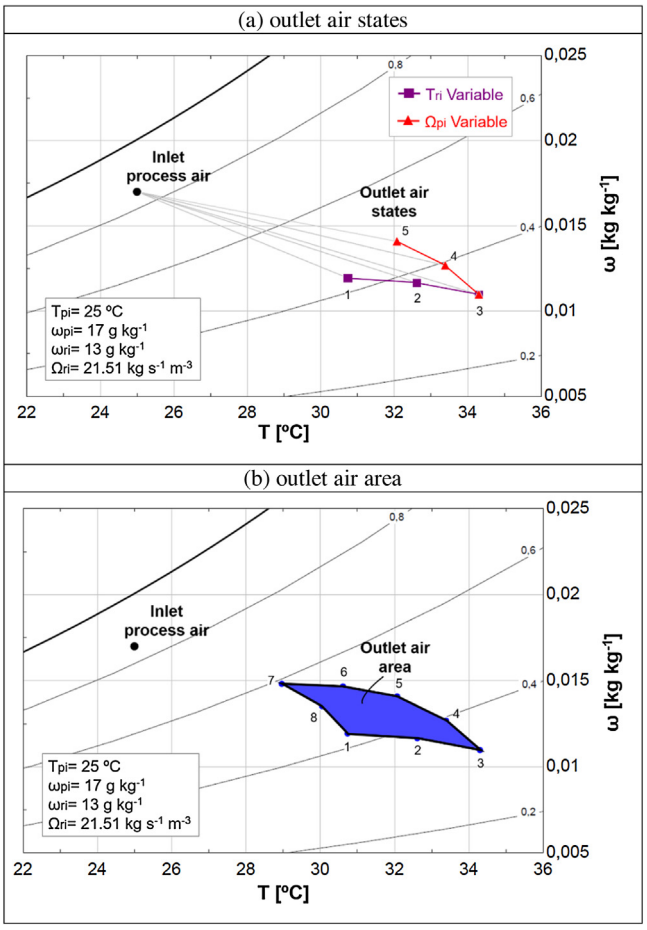

Fig. 5. Outlet process air conditions for case study I when T_{ri} and Ω_{pi} were varied.

3. Results and analysis

3.1. Experimental case study I

Experimental tests were carried out to analyse the variation of outlet process air conditions in a DW controlling T_{ri} and Ω_{pi}. The results of the outlet process air conditions of the DW for case study I are shown in Fig. 5. States 1 to 3 show the outlet air states when T_{ri} was varied from 34 °C to 42.5 °C, tests 1 to 3, see Table 7, and the remaining input variables were fixed at constant values, see Fig. 5a. States 3 to 5 show the outlet air states when Ω_{pi} was varied from 21.51 kg s^{-1} m^{-3} to 13.45 kg s^{-1} m^{-3}, test 3 to 5, see Table 7, and the remaining input variables were fixed at constant values, see Fig. 5a. These outlet process air states are shown in Table 10. It can be observed that T_{po}' increased and ω_{po}' decreased when T_{ri} and Ω_{pi} were increased, although different slopes were obtained.

The combination between the values of T_{ri} and Ω_{pi} defined in Table 7, resulted in an area of outlet process air, see Fig. 5b. The area obtained is equal to 8.26 °C g kg^{-1}. Any air state within the shaded area can be obtained by setting the T_{ri} and Ω_{pi} values in the specified range and fixing T_{pi}, ω_{pi}, ω_{ri} and Ω_{ri} at constant values, as shown in Table 7. The variations of the outlet air process temperature and humidity ratio from a fixed inlet state were 5.33 °C and 3.85 g kg^{-1}, respectively, see Table 10. These results show that this strategy allows the outlet process air conditions to be controlled in a DW setting T_{ri} and Ω_{pi}. Similar results can be obtained experimentally from different inlet process air states. In general, it is possible to vary the outlet process air conditions in a DW activated at low temperatures controlling T_{ri} and Ω_{pi}.

Table 10
Outlet process air conditions and MRC and SHR values obtained for case study I.

N	T_{po}' [°C]	ω_{po}' [g kg^{-1}]	MRC [kg h^{-1}]	SHR
1	30.74	11.93	9.37	0.70
2	32.61	11.66	9.81	0.68
3	34.3	10.97	11.04	0.64
4	33.38	12.68	7.92	0.74
5	32.07	14.09	5.36	0.82
6	30.61	14.67	4.31	0.86
7	28.97	14.82	4.06	0.87
8	30.05	13.53	6.43	0.79

3.2. Correlation model

An empirical model was obtained to predict the outlet air process temperature and humidity ratio, in order to control MRC and SHR in a DW operating at low air-regeneration temperatures.

The results of the set of experiments were used to fit the parameters of a second order model expressed by Eq. (1). The corresponding estimated parameters, which show the relationship between the output process variables, T_{po}' and ω_{po}', and the set of process variables, are shown in Table 11. Where X_i are linear variables, quadratic variables or their interactions, $b_1 \ldots b_{15}$ are the regression coefficients, showing the weight each one has in the equation, and b_0 is the average response in the design of experiments. It can be observed that the coefficients with the highest weight were b_2 for T_{po}', and b_3 for ω_{po}', ω_{pi} and T_{ri} variables, respectively.

3.2.1. Statistical analysis

The ANOVA results of the empirical model obtained are summarized in Table 12. This table shows each of the main estimated effects, the standard error of each of the effects, the statistical parameter F-Ratio, which is the ratio of the mean square error to the pure error obtained from the replicates at the design center, and the statistical parameter P-value, which is used as a tool to check the significance of each effect.

All variables were found significant at 95% confidence level, as the P-values were lower than 0.05 in all cases. The results of the parameter P-value showed that the most influential variables on the outlet temperature, T_{po}', were T_{pi}, T_{ri} and Ω_{pi}. Regarding the outlet humidity ratio, ω_{po}', the most influential variables were ω_{pi}, Ω_{pi}, and ω_{ri}. This suggested that if a fine tuning of outlet process air conditions was necessary, the process specific mass airflow, Ω_{pi}, should be controlled. Previous results of a DW with balanced airflow rates differ from the results obtained in this work [40], where the specific mass airflow presented less influence compared to the inlet air process and regeneration conditions.

Table 11
Estimated parameters of the empirical model.

Estimated parameters	X_i	T_{po}'x10^3 [°C]	ω_{po}'x10^3 [g kg^{-1}]	Estimated parameters	X_i	T_{po}'x10^3 [°C]	ω_{po}'x10^3 [g kg^{-1}]
b_0	–	−6736.67	−15366.80	b_{11}	ω_{pi}^2	−17.23	16.76
b_1	T_{pi}	72.10	1277.57	b_{12}	$\omega_{pi}\cdot T_{ri}$	−1.49	−2.23
b_2	ω_{pi}	772.28	−785.18	b_{13}	$\omega_{pi}\cdot\omega_{ri}$	5.65	16.84
b_3	T_{ri}	410.38	1310.33	b_{14}	$\omega_{pi}\cdot\Omega_{pi}$	20.50	−6.79
b_4	ω_{ri}	224.17	−916.88	b_{15}	T_{ri}^2	−5.09	−11.90
b_5	Ω_{pi}	357.36	−94.71	b_{16}	$T_{ri}\cdot\omega_{ri}$	7.31	−10.40
b_6	T_{pi}^2	16.58	−28.38	b_{17}	$T_{ri}\cdot\Omega_{pi}$	6.71	−3.50
b_7	$T_{pi}\cdot\omega_{pi}$	−14.35	29.84	b_{18}	ω_{ri}^2	−9.72	24.41
b_8	$T_{pi}\cdot T_{ri}$	7.35	−10.61	b_{19}	$\omega_{ri}\cdot\Omega_{pi}$	−5.49	11.88
b_9	$T_{pi}\cdot\omega_{ri}$	−12.93	6.35	b_{20}	Ω_{pi}^2	−12.17	−9.44
b_{10}	$T_{pi}\cdot\Omega_{pi}$	−8.71	5.89	–	–	–	–

Table 12
Effects of input variables on output process variables of the DW.

	T_{po}'				ω_{po}'			
Effect	Estimate	Stnd. Error	F-Ratio	P-value	Estimate	Stnd. Error	F-Ratio	P-value
Average	30.37	0.09			13.27	0.17		
T_{pi}	6.12	0.35	299.24	0.0000	3.04	0.63	23.07	0.0049
ω_{pi}	2.46	0.36	46.21	0.0010	5.44	0.65	70.06	0.0004
T_{ri}	3.54	0.21	281.66	0.0000	−1.12	0.38	8.95	0.0304
ω_{ri}	−1.39	0.21	43.66	0.0012	1.81	0.38	23.14	0.0048
Ω_{pi}	1.85	0.21	77.37	0.0003	−2.60	0.38	47.71	0.0010
Lack-of-fit				0.0600				0.0590
	R^2 = 98.23%				R^2 = 95.54%			

Positive and negative effects for the different input variables were observed, see Table 12. These signs indicate the influential trend of the input variables on the output process variables. T_{po}' can be increased, reducing ω_{ri} and increasing T_{pi}, ω_{pi}, T_{ri} and Ω_{pi}, and ω_{po}' can be increased, reducing T_{ri} and Ω_{pi} and increasing T_{pi}, ω_{pi} and ω_{ri}.

P-values for lack-of-fit test for T_{po}' and ω_{po}' were greater than 0.05, see Table 12. Therefore, the selected design was found suitable for the observed data at 95% confidence level. R^2 values of 98.23% for T_{po}' and 95.54% for ω_{po}' were obtained, which indicates that the final prediction is in agreement with the experimental results. In a previous work, where an empirical model of DW with bypass air was fitted, lower R^2 values were found, 90% for T_{po}' and 92% for ω_{po}' [41].

3.2.2. *Effect of input variables on the outlet process air conditions*

In order to find the relationships between input and output variables, two response surfaces and contour line plots for the output process variables, T_{po}' and ω_{po}', were analysed using the empirical model obtained, see Fig. 6. Both output process variables are represented as a function of the input variables T_{ri} and Ω_{pi}. The remaining input variables were fixed at constant values: T_{pi} = 27.25 °C, ω_{pi} = 16.75 g kg^{-1} and ω_{ri} = 16.75 g kg^{-1}. Similar trends of T_{po}' and ω_{po}' were obtained for different values of T_{pi}, ω_{pi} and ω_{ri}. It can be observed that T_{po}' increased when T_{ri} was increased and Ω_{pi} remained constant. T_{po}' values also increased when Ω_{pi} was increased and T_{ri} remained constant, see Fig. 6a. Inverse trends of these two input variables were obtained for ω_{po}'. Values of this output variable were increased when T_{ri} and Ω_{pi} decreased. In previous studies on DW with balanced airflow rates, similar trends of the output variables with regard to T_{ri}, were obtained [40,42]. However, inverse trends of the output process variables with regard to Ω_{pi} were achieved, where ω_{po}' values increased [1] and T_{po}' values decreased [42], as process airflow rates were increased. These trends are caused by the fact that the outlet process air conditions of the current DW system, were mixed with the bypass airflow and also, the regeneration and process airflow rates were unbalanced.

The effects of interaction between T_{ri} and Ω_{pi}, and T_{po}' and ω_{po}', using the empirical model obtained, were studied for three levels of T_{ri} and three levels of Ω_{pi}, see Table 8. Both effects are represented in Fig. 7. The same constant values of T_{pi}, ω_{pi} and ω_{ri}, as those shown in Fig. 6, were used. Low increments of T_{po}' can be observed when Ω_{pi} was increased and T_{ri} was fixed at a constant value, see Fig. 7a. For example, an increase of Ω_{pi} from 13.45 kg s^{-1} m^{-3} to 17.48 kg s^{-1} m^{-3}, and T_{ri} = 34 °C, yielded a lower increase of 1 °C for T_{po}'. With respect to ω_{po}', it can be observed that this output variable increased when Ω_{pi} decreased and T_{ri} was fixed at a constant value, see Fig. 7a. An increment of 1.4 g kg^{-1} for ω_{po}' was achieved when Ω_{pi} decreased from 17.48 kg s^{-1} m^{-3} to 21.51 kg s^{-1} m^{-3}, and T_{ri} = 34 °C.

Greater increments of T_{po}' were obtained when T_{ri} was increased and Ω_{pi} was fixed at a constant value, see Fig. 7b. A rise of approximately 2 °C of T_{po}' was achieved for each level of T_{ri} and Ω_{pi} = 13.45 kg s^{-1} m^{-3}. Regarding ω_{po}', lower increments of this output variable were found after fixing the Ω_{pi} at a constant value and varying T_{ri}, see Fig. 7b. For example, an increase of T_{ri} from 38.25 °C to 42.5 °C, and Ω_{pi} = 13.45 kg s^{-1} m^{-3}, yielded a lower increase of 1 g kg^{-1} for ω_{po}'. The maximum and minimum values of T_{po}' achieved were 35.5 °C and 29.8 °C, respectively, and the maximum and minimum values of ω_{po}' achieved were 15.4 g kg^{-1} and 11.3 g kg^{-1}, respectively. Similar trends of T_{po}' and ω_{po}' on T_{ri} and Ω_{pi} were obtained for different values of T_{pi}, ω_{pi} and ω_{ri}.

These results suggested that the influence of Ω_{pi} on T_{po}' was less than that of T_{ri}. Also, the influence of T_{ri} on ω_{po}' was less than that of Ω_{pi}. Therefore, a wider range of outlet process air conditions can be achieved if the outlet air temperature, T_{po}', is controlled by the inlet air regeneration temperature, T_{ri}, and the outlet air humidity ratio, ω_{po}', is controlled by the process specific mass airflow rate, Ω_{pi}. This strategy can be used to ensure independent control of outlet air temperature and humidity ratio.

3.3. *Analysis of outlet process air conditions for case study II*

The empirical model was used to analyse the variation of outlet process air conditions in the DW system for five inlet air states, states P1-P5. First, the outlet process air conditions were studied

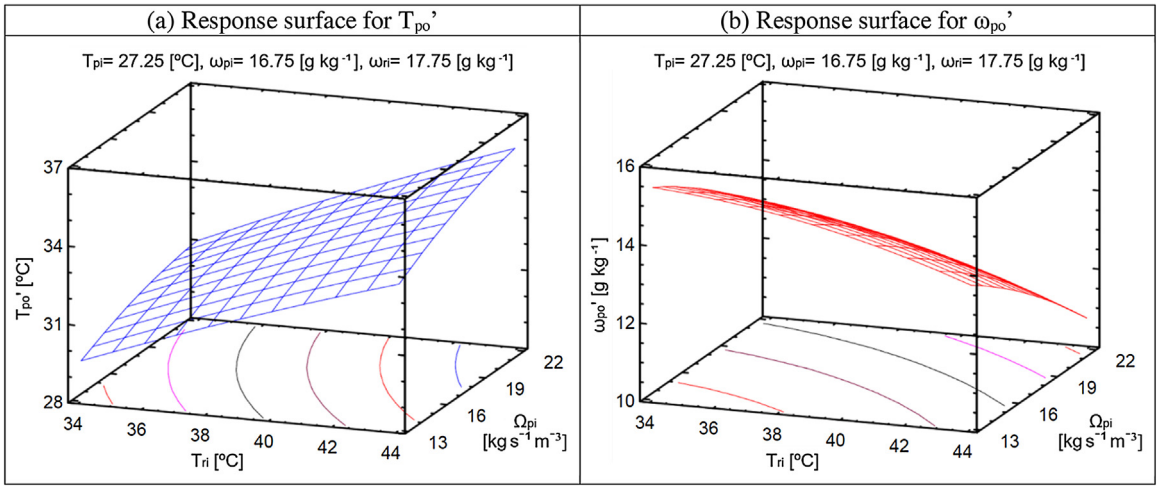

Fig. 6. Response surfaces and contour line plots of the output process variables.

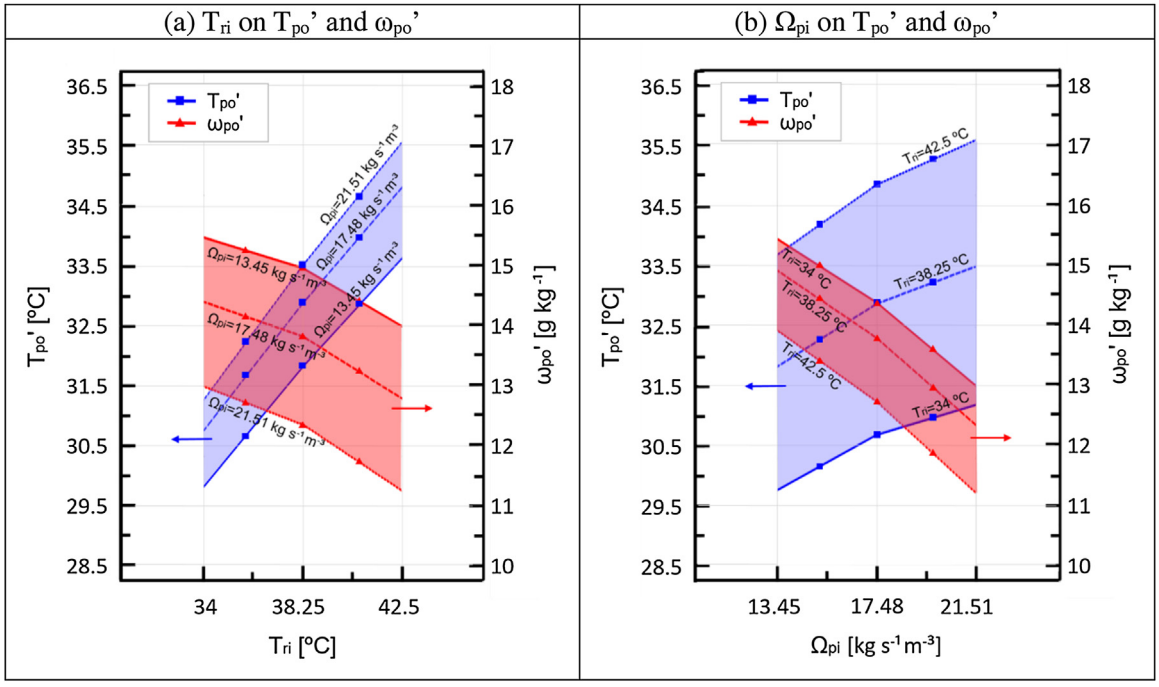

Fig. 7. Relations of T_{ri} and Ω_{pi} on T_{po}' and ω_{po}'.

when T_{ri} and ω_{ri} were varied. The combination of these two input variables are shown in Table 8. Ω_{pi} and Ω_{ri} were fixed at a constant value, 21.51 kg s^{-1} m^{-3}. The results of the outlet process air conditions are represented in Fig. 8. States P1 to P5 indicate the inlet process air conditions and the lines represent the outlet process air states. Three outlet process air lines for each inlet air state were obtained by varying ω_{ri}, and three outlet process air states were obtained in each outlet process air line by varying T_{ri}. Therefore, a decoupling of the outlet air process temperature and humidity was not completely achieved. Regarding ω_{ri}, ω_{po}' values were increased and T_{po}' values were reduced when ω_{ri} increased. Previous works showed that if extremely dry outlet process air conditions were necessary, the inlet air regeneration humidity ratio, ω_{ri}, should not be very high [40].

Second, in this case study, the outlet process air conditions were analysed when T_{ri}, Ω_{pi} and ω_{ri} were varied. The combination of these three input variables is shown in Table 8. The results of the

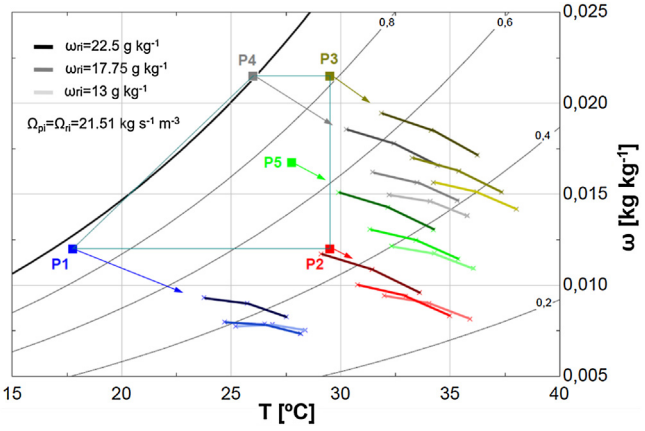

Fig. 8. Outlet process air conditions when T_{ri} and ω_{ri} were modified.

Table 13
Output area values for each inlet process air state, P1-P5.

ω_{ri} [g kg^{-1}]	P1 Area [°C g kg^{-1}]	P2 Area [°C g kg^{-1}]	P3 Area [°C g kg^{-1}]	P4 Area [°C g kg^{-1}]	P5 Area [°C g kg^{-1}]
13.00	8.80	8.25	7.45	7.96	8.10
17.75	7.53	7.17	6.06	6.24	7.00
22.50	6.46	6.09	4.37	4.72	5.28

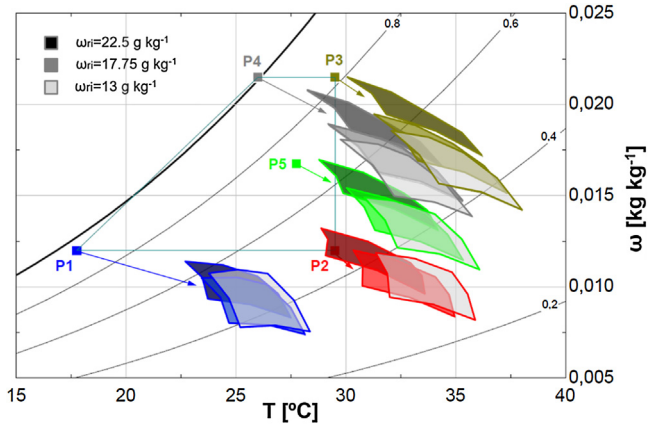

Fig. 9. Outlet process air conditions when T_{ri}, Ω_{pi} and ω_{ri} were modified.

Table 14
Area ratio values for the three input process areas and three levels of ω_{ri}.

ω_{ri} [g kg^{-1}]	Area Ratio I	Area Ratio II	Area Ratio III
13.00	2.35	2.53	2.89
17.75	2.40	2.59	2.95
22.50	2.46	2.63	3.03

outlet process air conditions are represented in Fig. 9. Three outlet process air areas were obtained for each inlet process air state by varying ω_{ri}. The decoupling of the temperature and humidity is shown by setting the T_{ri} and Ω_{pi}. Area values obtained from the contour of the outlet process air states, for each inlet process air state, P1-P5, are shown in Table 13. It can be observed that the greatest areas were achieved for inlet process air states with low ω_{pi} values, states P1 and P2. The areas were reduced when ω_{pi} increased, from states P1 and P2 to states P3 and P4, and the inlet process air conditions are located away from the saturation conditions, states P4 to P3 or states P1 to P2. Furthermore, the areas were reduced for all inlet process air states when ω_{ri} increased, from 13 to 22.5 g kg^{-1}, see Table 13.

Regarding the outlet process air area of state P2 with ω_{ri} = 22.5 g kg^{-1}, some outlet process air states with lower T_{po}' values and higher ω_{po}' values than the inlet air state, P2, were achieved, see Fig. 9. The proximity of T_{pi} to T_{ri}, and the relative high ω_{ri} values compared to the ω_{pi} values, caused this process.

3.4. Analysis of outlet process air conditions for case study III

The results of the outlet process air conditions of the DW system, for the three inlet process air conditions related to climatic conditions selected in Fig. 4, are shown in Fig. 10. Three output process areas were obtained for each input process area by varying ω_{ri}. These output process areas represent the set of individual outlet process air areas obtained from all inlet air states. The area ratio values, AR, for all output process areas, obtained by Eq. (2), are summarized in Table 14 and the increases of outlet air temperature and humidity ratio, ΔT_{po} and $\Delta\omega_{po}$, for each output area, are shown in Table 15. The results show that the AR values were increased when T_{pi} increased, from area I to area II, whose input process

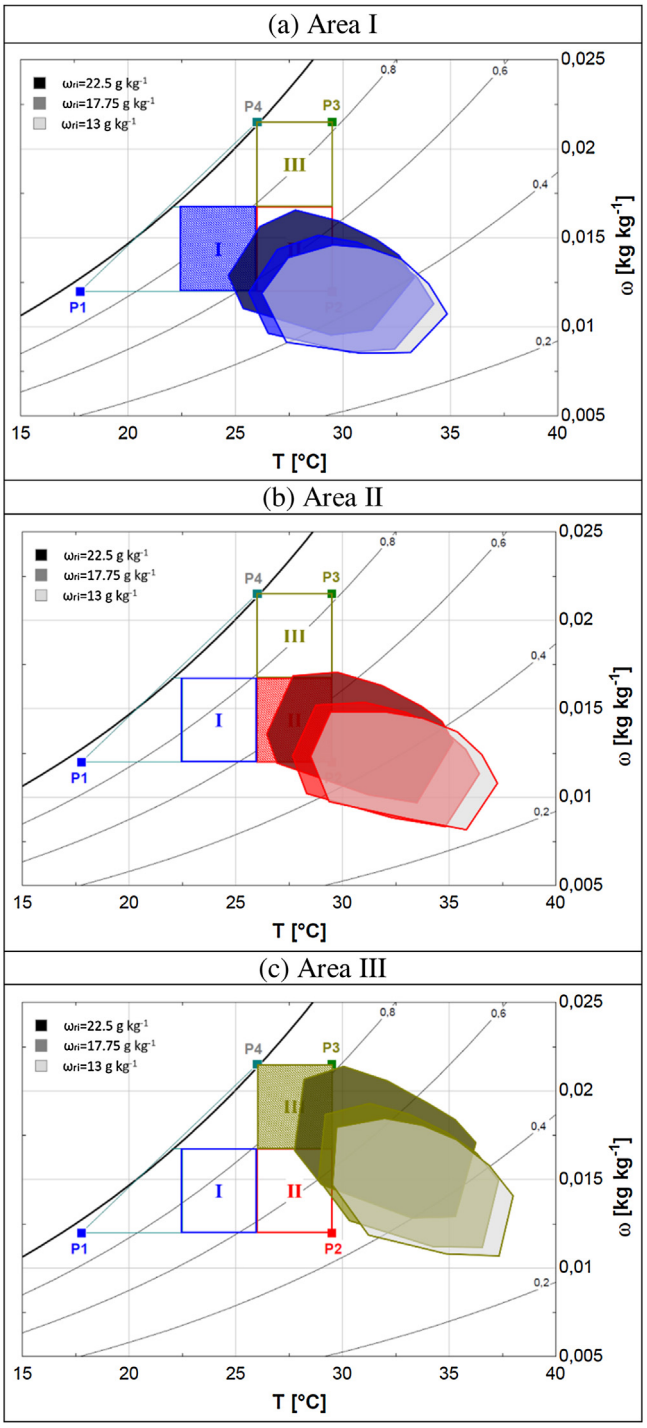

Fig. 10. Outlet process air conditions for the three input process areas when T_{ri}, Ω_{pi} and ω_{ri} were varied.

Table 15
Values of ΔT_{po} and $\Delta\omega_{po}$ for the three output process areas and three levels of ω_{ri}.

ω_{ri} [g kg^{-1}]	Outlet process air conditions					
	Area I		Area II		Area III	
	ΔT_{po} [°C]	$\Delta\omega_{po}$ [g kg^{-1}]	ΔT_{po} [°C]	$\Delta\omega_{po}$ [g kg^{-1}]	ΔT_{po} [°C]	$\Delta\omega_{po}$ [g kg^{-1}]
13.00	8.59	6.07	8.74	6.66	8.53	8.81
17.75	8.59	6.53	8.73	7.00	8.86	9.22
22.50	8.59	6.98	8.73	7.35	9.04	9.63

areas have the same inlet air humidity ratio range but different inlet air temperature range. The difference between area I and area II with respect to ΔT_{po} was 0.15 °C, and with respect to $\Delta\omega_{po}$ was less than 0.6 g kg^{-1}, see Table 15. In addition, the AR values were increased when ω_{pi} increased, from area II to area III, whose input process areas have the same inlet air temperature range but different inlet air humidity ratio range. The differences of ΔT_{po} and $\Delta\omega_{po}$ between area II and area III were less than 0.31 °C and 2.3 g kg^{-1} respectively, see Table 15. Thus, the maximum and minimum AR values were achieved for area III and area I, respectively.

Regarding ω_{ri}, it can be observed that the AR values were increased when ω_{ri} increased, see Table 14. This trend is inverse to that obtained with fixed inlet process air states, case study II. This is caused by the fact that in case study II each outlet process air state corresponds to a single inlet process air state. However, in case study III each outlet process air state corresponds to several inlet process air states.

These results suggest that the higher the T_{pi}, ω_{pi} and ω_{ri} values, the larger the area of outlet process air conditions.

3.5. Analysis of moisture removal capacity and sensible heat ratio

The variation of the outlet process air conditions from a given inlet process air state, by setting the T_{ri} and Ω_{pi}, caused MRC and SHR values to be modified. The MRC and SHR values of the process air stream for case study I were obtained experimentally, see Table 10. MRC ranged from 4.06 to 11.04 kg h^{-1}. The highest MRC value was obtained at the lower part of the outlet process air area, state 3 defined in Table 7, i.e. for the highest T_{ri} and Ω_{pi} value. SHR ranged from 0.64 to 0.87, where the highest SHR value was obtained at the upper part of the outlet process air area, state 7 defined in Table 7, i.e. for the lowest T_{ri} and Ω_{pi} value.

Regarding case study III, MRC and SHR values were not obtained, because for different inlet process air states, several MRC and SHR values exist in the same outlet process air state.

Regarding case study II, the MRC and SHR values of the process air stream for the five inlet air states, P1-P5, were obtained from the empirical model, and the results are represented in Fig. 11. The differences of MRC between the lower and upper part of the outlet air area were approximately 7 kg h^{-1} for all inlet process air states, see Fig. 11a. The highest MRC values were obtained at the lower part of the outlet process air area. These results of MRC are in agreement with those obtained in experimental case study I. On the other hand, the results showed that the increase of MRC was inversely proportional to the increase of outlet process air area, A_o. The MRC maximum value was achieved for P4 outlet air area, approximately 14 kg h^{-1}, where high ω_{pi} values and inlet air conditions close to saturation, were fixed. This moisture removal capacity was acceptable compared to the MRC nominal value, 15 kg h^{-1}, see Table 2, where the DW was activated at high regeneration temperatures.

The differences of SHR between the lower and upper part of the outlet air area were approximately 0.25 for all inlet process air states, see Fig. 11b. The lowest SHR values were obtained at the lower part of the outlet process air area. These results of SHR are in agreement with those obtained in experimental case study I. The SHR minimum value was achieved for P1 outlet air area, approximately 0.62.

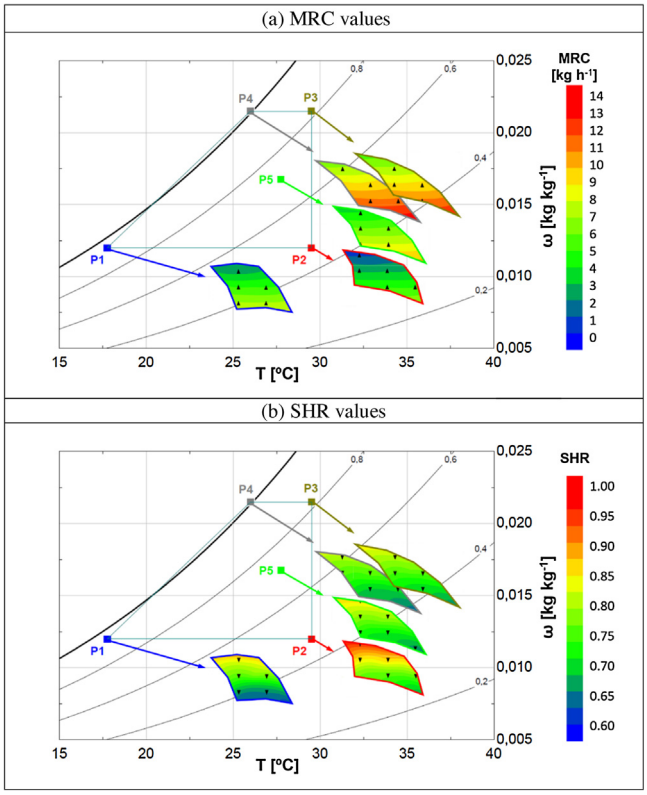

Fig. 11. MRC and SHR values of the five inlet air states for case study II.

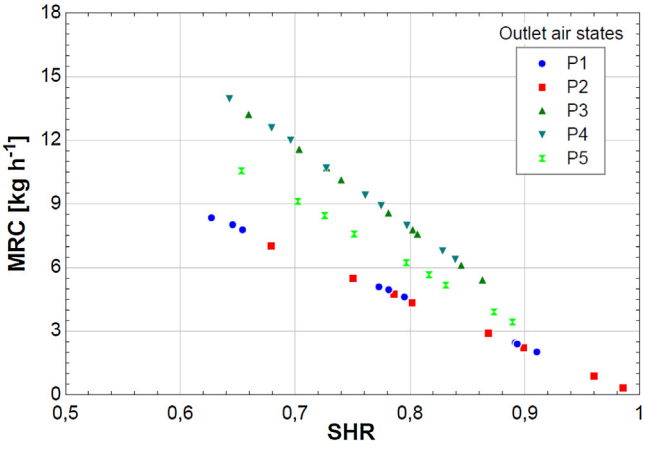

Fig. 12. Relationship between MRC and SHR for case study II.

The relationships between MRC and SHR for the five inlet air states, P1-P5, were obtained using the empirical model, as shown in Fig. 12. Similar slopes were obtained for equal ω_{pi} values, P1-P2

and P3-P4. However, for the same slope angle, the MRC values were increased and the SHR values were reduced when T_{pi} decreased, P2 to P1 and P3 to P4. It can be observed that the slope angle of the MRC-SHR relationship was higher when ω_{pi} increased. Furthermore, for the same MRC values, the SHR values were increased when ω_{pi} increased.

These results suggest that a control strategy by setting T_{ri} and Ω_{pi}, would allow MRC and SHR to be controlled over a wide range of outlet process air conditions of a DW activated at low temperatures. Furthermore, these results show a significant influence of the inlet air process humidity ratio on the MRC-SHR relationship. Therefore, different MRC-SHR relationships can be obtained by adjusting the inlet air process humidity ratio.

4. Conclusions

In the present work, an analysis of MRC and SHR of a DW activated at low temperatures, values below 60 °C, by varying the process airflow rate and air regeneration temperature, was carried out. Case study I was tested experimentally and case studies II and III were carried out using an empirical model fitted with the statistical technique of design of experiments, DOE. This empirical model allowed the analysis of the outlet process air conditions for a wide range of inlet air states.

The experimental and simulated results showed that a decoupling of the outlet process air conditions, temperature and humidity ratio, can be obtained when the process airflow rate and air regeneration temperature are varied. This decoupling resulted in a psychrometric area of the outlet process air. The outlet process air area was increased when inlet process air conditions were located close from saturation and the inlet air process and regeneration humidity ratio values were reduced. The maximum and minimum values of outlet process air area achieved from a given inlet process air state were 8.80 °C g kg^{-1} and 4.37 °C g kg^{-1}, respectively. Furthermore, a wider range of the outlet process air area can be achieved if the outlet air process temperature is controlled by the inlet air regeneration temperature, and the outlet air process humidity ratio is controlled by the process specific mass airflow rate. These results suggest that a control strategy by setting the process airflow rate and air regeneration temperature, would allow MRC and SHR to be controlled over a wide range of outlet process air conditions for a DW activated at low temperatures.

MRC and SHR were obtained experimentally and numerically for the case studies. The differences of MRC and SHR between the lower and upper part of the outlet air area were approximately 7 kg h^{-1} and 0.25, respectively, for all inlet process air states The highest MRC values and the lowest SHR values were obtained for the highest process airflow rate values and the highest inlet air regeneration temperature values, 14 kg h^{-1} and 0.62, respectively. The relationship between MRC and SHR was analysed, where several MRC values were obtained for a constant SHR value and vice versa. A significant influence of the inlet air process humidity ratio on the MRC-SHR relationship was showed. Therefore, different relationships can be obtained by adjusting the inlet air process humidity ratio.

The results show that a DW system activated at low temperatures, by setting the process airflow rate and air regeneration temperature, can obtain an independent control of MRC and SHR.

Acknowledgements

This work is related to the research project dehumidification and air drying, DESSECA, promoted by the company CIAT and co-funded by the Agency for Innovation and Development of Andalusia, expedient IDEA 360097, and by the Technological Corporation of Andalusia, expedient CTA 12/612, (2012-2014). The authors are grateful for the collaboration of Adoración Cerezuela Parish and Dr. Miguel Zamora García from CIAT Spain R&I Department.

References

[1] L.G. Harriman III, The Dehumidification Handbook, 2nd ed., Munters Corp., Amesbury, MA, 2003.
[2] D. Shirey, H. Henderson, R. Raustad, Understanding the Dehumidification Performance of Air-Conditioning Equipment at Part-Load Conditions, 641, 2006, pp. 655–1063.
[3] Y. Sheng, Y. Zhang, N. Deng, L. Fang, J. Nie, L. Ma, Experimental analysis on performance of high temperature heat pump and desiccant wheel system, Energy Build. 66 (2013) 505–513.
[4] D.B. Jani, M. Mishra, P.K. Sahoo, Performance studies of hybrid solid desiccant-vapor compression air-conditioning system for hot and humid climates, Energy Build. 102 (2015) 284–292.
[5] N. Wang, J. Zhang, X. Xia, Desiccant wheel thermal performance modeling for indoor humidity optimal control, Appl. Energy 112 (2013) 999–1005.
[6] R. Tu, X.-H. Liu, Y. Jiang, Performance analysis of a two-stage desiccant cooling system, Appl. Energy 113 (2014) 1562–1574.
[7] D. La, Y.J. Dai, Y. Li, Z.Y. Tang, T.S. Ge, R.Z. Wang, An experimental investigation on the integration of two-stage dehumidification and regenerative evaporative cooling, Appl. Energy 102 (2013) 1218–1228.
[8] H. Li, Y.J. Dai, Y. Li, D. La, R.Z. Wang, Case study of a two-stage rotary desiccant cooling/heating system driven by evacuated glass tube solar air collectors, Energy Build. 47 (2012) 107–112.
[9] C.R. Ruivo, F. Fernández Hernández, J.M. Cejudo López, Influence of the desiccant wheel effectiveness method approaches with fix and variable effectiveness parameters, on the performance results of an airport air-conditioning system, Energy Convers. Manag. 94 (2015) 458–471.
[10] L. Yadav, A. Yadav, Mathematical investigation of purge sector angle for clockwise and anticlockwise rotation of desiccant wheel, Appl. Therm. Eng. 93 (2016) 839–848.
[11] U. Eicker, U. Schürger, M. Köhler, T. Ge, Y. Dai, H. Li, et al., Experimental investigations on desiccant wheels, Appl. Therm. Eng. 42 (2012) 71–80.
[12] G. Angrisani, C. Roselli, M. Sasso, Effect of rotational speed on the performances of a desiccant wheel, Appl. Energy 104 (2013) 268–275.
[13] S. De Antonellis, M. Intini, C.M. Joppolo, F. Romano, On the control of desiccant wheels in low temperature drying processes, Int. J. Refrig. 70 (2016) 171–182.
[14] M. Aprile, M. Motta, Grey-box modelling and in situ experimental identification of desiccant rotors, Appl. Therm. Eng. 51 (2013) 55–64.
[15] A.G.C.C. American Gas Cooling Center, in: Applications Engineering Manual for Desiccant Systems, Arlington, TX, 1996.
[16] M. Intini, S. De Antonellis, C.M. Joppolo, The effect of inlet velocity and unbalanced flows on optimal working conditions of silica gel desiccant wheels, Energy Procedia 48 (2014) 858–864.
[17] S.D. White, M. Goldsworthy, R. Reece, T. Spillmann, A. Gorur, D.Y. Lee, Characterization of desiccant wheels with alternative materials at low regeneration temperatures, Int. J. Refrig. 34 (2011) 1786–1791.
[18] S. De Antonellis, M. Intini, C.M. Joppolo, Desiccant wheels effectiveness parameters: correlations based on experimental data, Energy Build. 103 (2015) 296–306.
[19] C.R. Ruivo, M. Goldsworthy, M. Intini, Interpolation methods to predict the influence of inlet airflow states on desiccant wheel performance at low regeneration temperature, Energy 68 (2014) 765–772.
[20] C.R. Ruivo, A. Carrillo-Andres, J.J. Costa, F. Dominguez-Munoz, Exponential correlations to predict the dependence of effectiveness parameters of a desiccant wheel on the airflow rates and on the rotation speed, Appl. Therm. Eng. 51 (2013) 442–450.
[21] E. Kozubal, J. Woods, J. Burch, A. Boranian, T. Merrigan, Desiccant Enhanced Evaporative Air-Conditioning (DEVap): Evaluation of a New Concept in Ultra Efficient Air Conditioning, Technical Report NREL/TP-5500-49722, 2011.
[22] M.A. Sayegh, M. Hammad, Z. Faraa, Comparison of two methods of improving dehumidification in air conditioning systems: hybrid system (refrigeration cycle – Rotary desiccant) and heat exchanger cycle, Energy Procedia 6 (2011) 759–768.
[23] J. Jeong, S. Yamaguchi, K. Saito, S. Kawai, Performance analysis of four-partition desiccant wheel and hybrid dehumidification air-conditioning system, Int. J. Refrig. 33 (2010) 496–509.
[24] G. Angrisani, F. Minichiello, C. Roselli, M. Sasso, Experimental analysis on the dehumidification and thermal performance of a desiccant wheel, Appl. Energy 92 (2012) 563–572.
[25] J.D. Chung, D.Y. Lee, S.M. Yoon, Optimization of desiccant wheel speed and area ratio of regeneration to dehumidification as a function of regeneration temperature, Sol. Energy 83 (2009) 625–635.
[26] Y. Sheng, Y. Zhang, Y. Sun, L. Fang, J. Nie, L. Ma, Experimental analysis and regression prediction of desiccant wheel behavior in high temperature heat pump and desiccant wheel air-conditioning system, Energy Build. 80 (2014) 358–365.
[27] D.B. Jani, M. Mishra, P.K. Sahoo, Performance prediction of rotary solid desiccant dehumidifierin hybrid air-conditioning system using artificial neural network, Appl. Therm. Eng. 98 (2016) 1091–1103.

[28] Y. Guan, Y. Zhang, Y. Sheng, X. Kong, S. Du, Feasibility and economic analysis of solid desiccant wheel used for dehumidification and preheating in blast furnace: a case study of steel plant Nanjing, China, Appl. Therm. Eng. 81 (2015) 426–435.
[29] C.E.L. Nóbrega, N.C.L. Brum, An analysis of the heat and mass transfer roles in air dehumidification by solid desiccants, Energy Build. 50 (2012) 251–258.
[30] F. Comino, M. Ruiz de Adana, F. Peci, Experimental study of the moisture removal capacity of a desiccant wheel activated at low and high temperature, CLIMA 2016, Aalborg University, Department of Civil Engineering, in: Proc. 12th REHVA World Congress, vol. 9, 2016.
[31] J. Wrobel, P. Morgenstern, G. Schmitz, Modeling and experimental validation of the desiccant wheel in a hybrid desiccant air conditioning system, Appl. Therm. Eng. 51 (2013) 1082–1091.
[32] S. De Antonellis, C.M. Joppolo, L. Molinaroli, A. Pasini, Simulation and energy efficiency analysis of desiccant wheel systems for drying processes, Energy 37 (2012) 336–345.
[33] C.R. Ruivo, A. Carrillo-Andrés, J.J. Costa, F. Domínguez-Muñoz, Interpolation procedures for the effectiveness method to account for the influence of the inlet airflow states on the desiccant wheels performance, Energy Build. 55 (2012) 380–388.
[34] A.M. Baniyounes, M.G. Rasul, M.M.K. Khan, Experimental assessment of a solar desiccant cooling system for an institutional building in subtropical Queensland Australia, Energy Build. 62 (2013) 78–86.
[35] F. Comino Montilla, M. Ruiz de Adana Santiago, A. Cerezuela Parish, M. Zamora García, F. Peci López, Design and building of a test facility for experimentation of desiccant wheels, in: the Minutes Book of the National Congress Engineering Thermodynamics, Cartagena (2015) 295–302.
[36] D.C. Montgomery, Design and Analysis of Experiments, sixth ed., Wiley, New York, 2004.
[37] Statgraphics Centurion XV, 2006, available from http://www.statgraphics.com/(accessed 15.05.16).
[38] C.R. Ruivo, A. Carrillo-Andrés, J.J. Costa, F. Domínguez-Muñoz, A new approach to the effectiveness method for the simulation of desiccant wheels with variable inlet states and airflows rates, Appl. Therm. Eng. (2012) 1–9.
[39] ASHRAE, Method of Testing for Rating Desiccant Dehumidifiers Utilizing Heat for the Regeneration Process, ASHRAE standard, 2007.
[40] F. Comino, M.R. de Adana, F. Peci, First and second order simplified models for the performance evaluation of low temperature activated desiccant wheels, Energy Build. 116 (2016) 574–582.
[41] M. Beccali, R.S. Adhikari, F. Butera, V. Franzitta, Update on desiccant wheel model, Int. J. Energy Res. 28 (2004) 1043–1049.
[42] F.E. Nia, Sustainable Air Handling by Evaporation and Adsorption, Deft University of Technology, PhD thesis, 2011.